



1 **Description of the China global Merged Surface**
2 **Temperature version 2.0**

3 Wenbin Sun^{1,#}, Yang Yang^{1,#}, Liya Chao^{1,#}, Wenjie Dong^{1,#}, Boyin Huang², Phil Jones³,

4 Qingxiang Li^{1,#}

5 ¹ *School of Atmospheric Sciences and Key Laboratory of Tropical Atmosphere-Ocean System, Sun Yat-sen University, Ministry of*
6 *Education, Guangzhou, China*

7 ² *National Centers of Environmental Information, NOAA, Asheville, USA*

8 ³ *Climate Research Unit, University of East Anglia, Norwich, UK*

9 [#] *Current address: Southern Laboratory of Ocean Science and Engineering (Guangdong Zhuhai), Zhuhai, China*

10 *Corresponding to: Qingxiang Li (liqingx5@mail.sysu.edu.cn)*

11

12 **Abstract.** Global surface temperature observational datasets are the basis of global warming studies.
13 In the context of increasing global warming and frequent extreme events, it is essential to improve
14 the coverage and reduce the uncertainty of global surface temperature datasets. The China global
15 Merged Surface Temperature Interim version (CMST-Interim) is updated to CMST 2.0 in this study.
16 The previous CMST datasets were created by merging the China global Land Surface Air
17 Temperature (C-LSAT) with sea surface temperature (SST) data from the Extended Reconstructed
18 Sea Surface Temperature version 5 (ERSSTv5). The CMST2.0 contains three variants: CMST2.0-
19 Nrec (without reconstruction), CMST2.0-Imax, and CMST2.0-Imin (According to their
20 reconstruction area of the air temperature over the sea ice surface in the Arctic region). The
21 reconstructed datasets significantly improve data coverage, whereas CMST2.0-Imax and CMST2.0-
22 Imin have improved coverage in the Northern Hemisphere, up to more than 95%, and thus increased
23 the long-term trends at global, hemispheric, and regional scales from 1850 to 2020. Compared to
24 CMST-Interim, CMST2.0-Imax and CMST2.0-Imin show a high spatial coverage extended to the
25 high latitudes and are more consistent with a reference of multi-dataset averages in the polar regions.
26 The CMST2.0 datasets presented here are publicly available at the website of figshare,
27 <https://doi.org/10.6084/m9.figshare.16929427.v4> (Sun and Li, 2021a) and the CLSAT2.0 datasets
28 can be downloaded at <https://doi.org/10.6084/m9.figshare.16968334.v4> (Sun and Li, 2021b).
29

30 **1. Introduction**

31 Global Surface Temperature (GST) is a key meteorological factor in characterizing climate
32 change and has been widely used for climate change detection and assessment (IPCC, 2013; 2021).
33 GST consists of global Land Surface Air Temperature (LSAT), which is the 2-m air temperature
34 observed by land weather stations, and Sea Surface Temperature (SST) observed by ships, buoys
35 and Argos. However, there are large uncertainties in the temperature data observed by weather
36 stations, ships, buoys and Argos in long-term observations, including uncertainties due to uneven
37 spatial and temporal distribution of sampling (Jones et al., 1997; Brohan et al., 2006) and



38 uncertainties due to stations, environment and instrumentation changes (Parker et al., 1994; Parker,
39 2006; Trewin, 2012; Kent et al., 2017; Menne et al., 2018; Xu et al., 2018). Nevertheless, several
40 countries and research teams have applied different homogenization methods to generate a series of
41 representative homogenized global land-sea surface temperature gridded datasets, including the Met
42 Office Hadley Centre/Climatic Research Unit Global Gridded Monthly Temperature (HadCRUT)
43 (Morice et al., 2012), Goddard Institute for Space Studies Surface Temperature (GISTEMP)
44 (Hansen et al., 2010; Lenssen et al., 2019), NOAA's NOAA Global Temperature
45 (NOAAGlobalTemp) (Vose et al., 2012; Zhang et al., 2019; Huang et al., 2020), and Berkeley Earth
46 (BE) (Rohde et al., 2013a; Rohde and Hausfather, 2020), which serve as benchmark data for
47 monitoring and detecting GST changes and related studies.

48 However, there are still uncertainties in these datasets, including those due to insufficient
49 coverage, especially at high altitudes and in the polar regions. The Arctic has high climate sensitivity
50 (Lu and Cai, 2009, 2010; Yamanouchi, 2011; Dai et al., 2019; Xiao et al., 2020; Latonin et al., 2021),
51 the absence of data for this region would lead to a cold bias in the estimated global mean surface
52 temperature (GMST). How to improve this deficiency is an issue that must be addressed to optimize
53 and improve the observations. Since IPCC AR5 (2013), all of the above datasets have been updated
54 and reconstructed in the data default region (IPCC, 2021). For example, Cowtan and Way (2014)
55 used kriging and hybrid methods to fill in the HadCRUT4 data gap areas, extending the data to polar
56 regions. GISTEMP v4 utilized spatial interpolation methods to fill in the default data within the
57 appropriate distances (1200km) (Lenssen et al., 2019). NOAA/NCEI used spatial smoothing and
58 empirical orthogonal remote correlations (EOTs) to reconstruct the data default areas, generating
59 100-member GHCN ensemble data and 1000-member ERSST ensemble data, respectively, which
60 were combined into the NOAAGlobalTemp-Interim dataset (Vose et al., 2021). HadCRUT team
61 infilled HadCRUT5 using the Gaussian process method (Morice et al., 2021). Kadow et al. (2020)
62 used artificial intelligence (AI) in combination with numerical climate model data to fill the
63 observation gaps in HadCRUT4. Berkeley Earth used kriging-based spatial interpolation to fill in
64 the terrestrial default data (Rohde et al., 2013a; Rohde et al., 2013b; Rohde and Hausfather, 2020).
65 Interpolation and reconstruction for high latitudes reduce the error in the estimate of GMST.
66 Compared to 0.61 (0.55-0.67) °C in IPCC AR5, GST warming estimated with reconstructed datasets
67 in AR6 from 1850-1800 to 1986-2005 is 0.69 (0.54-0.79) °C, which increased 0.08 (- 0.01 to
68 0.12) °C (IPCC, 2021).

69 China global Merged Surface Temperature (China-MST or CMST) is a new global surface
70 temperature dataset developed by the team at Sun Yat-sen University, which was merged by China
71 global Land Surface Air Temperature (China-LSAT or C-LAST) (Xu et al., 2018; Yun et al., 2019;
72 Li et al., 2020; Li et al., 2021) as the terrestrial component and ERSSTv5 (Extended Reconstructed
73 Sea Surface Temperature version 5) (Huang et al., 2017) as the ocean component. It is generally
74 consistent with other global datasets in terms of GST trends and uncertainty levels since 1880 (Li et
75 al., 2020). Compared with other datasets, the station coverage of C-LSAT has been significantly
76 improved, especially for Asia (Xu et al., 2018), and more ISTI station data have been added in C-
77 LSAT 2.0 (Li et al., 2021; Thorne et al., 2011). In addition, C-LSAT adopted a homogenization
78 scheme for temperature series that is different from datasets such as the Global Historical
79 Climatology Network version 4 (GHCNm v4) (Menne et al., 2018). Further, Sun et al. (2021) trained
80 EOTs modes with “state-of-the-art” ERA5 reanalysis data to extract the spatial distribution of LSAT.
81 They then used a similar low- and high-frequency reconstruction method of Huang et al. (2020)



82 with different parameter schemes, combined with the observation constraint method, to fill the data
83 default region of C-LSAT2.0 and released the new reconstructed dataset C-LSAT2.0 ensemble and
84 the global surface temperature dataset CMST-Interim. Compared with the original CMST, CMST-
85 Interim significantly improves the coverage of GST, and the GST warming estimated by CMST-
86 Interim is more significant, with the warming trend since the 1900s increasing from $0.085 \pm 0.004^{\circ}\text{C}$
87 $(10 \text{ yr})^{-1}$ to $0.089 \pm 0.004^{\circ}\text{C} (10 \text{ yr})^{-1}$. In the current CMST-Interim (Sun et al., 2021) and its earlier
88 version (Yun et al., 2019), we still fully adopted the setting from ERSSTv5, which treats the sea ice
89 region in the Arctic as the sea surface temperature below the sea ice and assigns a default value ($-$
90 1.8°C), which makes it still a gap in the polar region. In contrast, polar regions are susceptible to
91 climate forcing, with the Arctic warming more than twice the global average in recent decades
92 (Goosse et al., 2018). The lack of data from CMST-Interim in polar regions may result in a slight
93 underestimation of its estimated global warming trend. Furthermore, CMST-Interim does not
94 systematically assess the reconstruction uncertainty of LSAT, resulting in an incomplete estimate of
95 global surface temperature uncertainty (Li et al., 2021). Although C-LSAT 2.0 ensemble satisfied
96 the criterion of the recently released the 6th assessment report of IPCC, the CMST -Interim does not
97 appear in the core assessment GMST series due to its insufficient data coverage in the Arctic region
98 (Gulev et al, 2021).

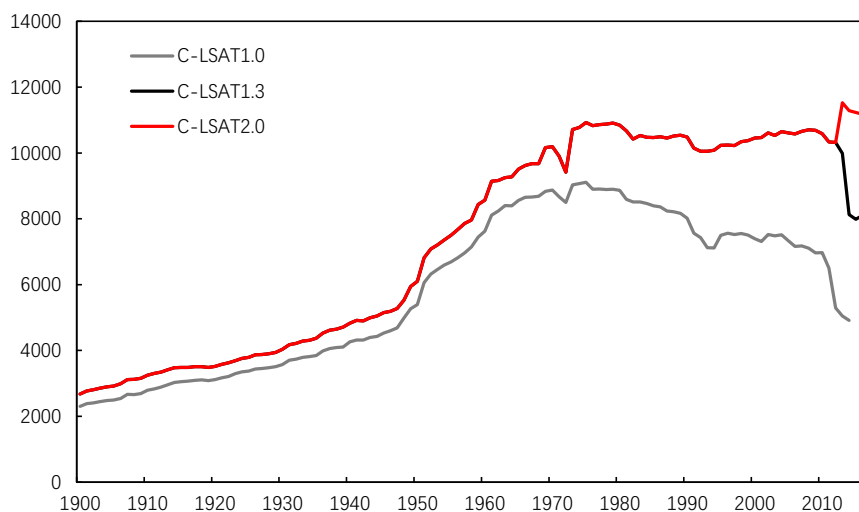
99 To address the above issue and improve coverage of CMST in the Arctic, we further reconstruct
100 and supplement the Arctic data default region in the dataset using a combination of statistical
101 interpolation and high- and low-frequency reconstruction to develop the reconstructed CMST2.0
102 dataset and assess its uncertainty. Section 2 introduces the update of terrestrial and oceanic datasets,
103 section 3 presents the reconstruction and uncertainty analysis of CMST2.0, section 4 introduces the
104 composition of C-LSAT2.0 and CMST2.0, section 5 analyzes the GMST series of CMST2.0, section
105 6 is the comparison of CMST2.0 dataset with other datasets, section 7 provides the summary and
106 outlook, and section 8 is data availability.

107 2. Updates of the land and ocean datasets

108 2.1 Data sources and initial processing for C-LSAT2.0

109 The initial version of the C-LSAT dataset was C-LSAT1.0. The C-LSAT1.0 site dataset
110 collected and integrated 14 LSAT datasets, including three global data sources (CRUTEM4, GHCN-
111 V3, and BEST), three regional data sources, and eight national situ data sources (Xu et al., 2018).
112 The current latest version is C-LSAT 2.0 (Li et al., 2021; Sun et al., 2021).

113 C-LSAT 2.0 used in this study is an update of C-LSAT 1.3. Compared to C-LSAT 1.3 from
114 1900 to 2017, version 2.0 extend to 1850-2020, and there is a significant increase in the amount of
115 in situ data for the period 2013-2017 (Figure 1), with the increased situ data from CLIMAT from
116 WMO's Global Telecommunication System (GTS) and Global Surface Daily Summary (GSOD)
117 (<https://www.ncei.noaa.gov/data/global-summary-of-the-day/archive/>; last access: November 2021)
118 and is homogenized using the same method as Xu et al. (2018). In addition, we have updated the
119 data in C-LSAT2.0 for 2013-2019, which adds the number of situ data in Africa, North America and
120 other regions in this study. The C-LSAT 2.0 dataset includes three temperature elements: monthly
121 mean temperature, maximum temperature, and minimum temperature, and its time range for the
122 three elements is January 1850 - December 2020.



123

124

Figure 1 Comparison of C-LSAT 1.3 and C-LSAT 2.0 site counts from 1900 to 2017

125

2.2 Sea surface temperature

126

127

128

129

130

131

132

133

134

2.3 Sea ice surface air temperature

135

136

137

138

139

140

141

142

3. CMST2.0 reconstruction and uncertainty analysis

143

144

3.1 CMST and its brief reconstruction history

145

146

147

148

149

150

151

CMST 1.0 consists of C-LSAT 1.3 (1900-2017) as the terrestrial component and ERSSTv5 as the ocean component. The latest version without reconstruction is CMST2.0-Nrec in this study, which composes of C-LSAT2.0 and ERSSTv5. Compared to CMST1.0 from 1900-2017, CMST2.0-Nrec has been updated and expanded to 1850-2020. The original reconstructed version of CMST is the Chinese global merged surface temperature reconstruction dataset CMST-Interim, which is a merge of the reconstructed C-LSAT2.0 and ERSSTv5, where the reconstructed C-LSAT2.0 is an ensemble reconstruction dataset upgraded from C-LSAT2.0 (Li et al., 2021) with 756 ensemble



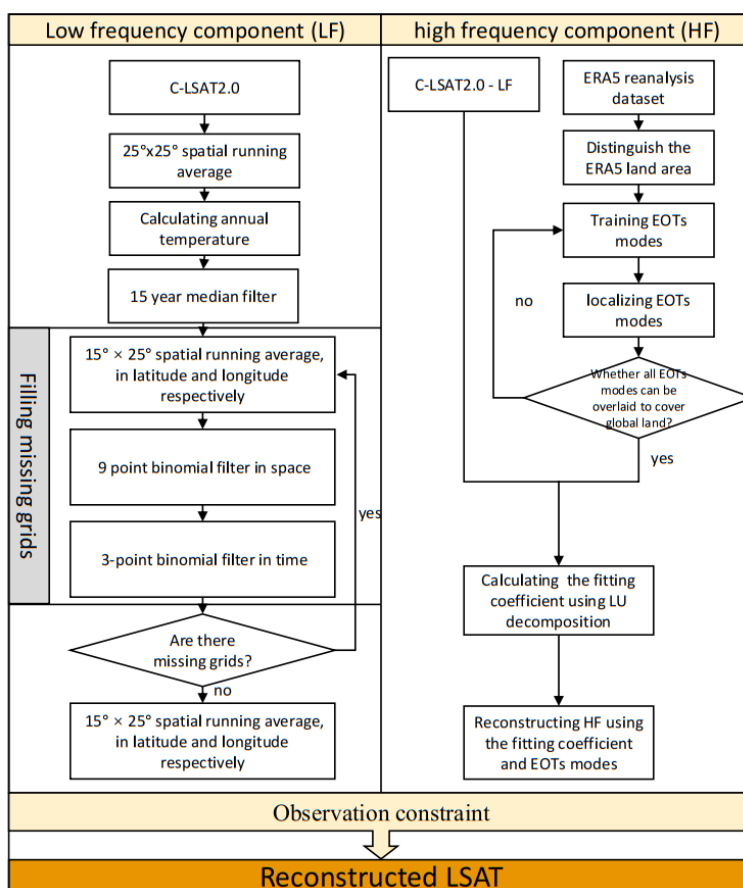
152 members identified based on EOT and smoothing (Sun et al., 2021). Considering that there are much
153 missing data due to sea ice coverage at high latitudes in the Northern Hemisphere in CMST, the
154 IDW extrapolation method is proposed to infill the missing data in some key sites, then EOT
155 interpolation method is used to reconstruct all the grid boxes over the sea-ice-covered region in this
156 paper. Considering the effect of interannual variability of sea ice in the Arctic, 65°N-90°N and 80°N-
157 90°N are taken as the assumed land components for ensemble reconstruction with C-LSAT 2.0,
158 respectively, using the maximum sea ice area and minimum sea ice area since satellite observations
159 are available as reference, then the ERSSTv5 ensemble reconstruction dataset is merged to generate
160 CMST 2.0-Imax and CMST 2.0-Imin datasets.

161 **3.2 Reconstruction of terrestrial and marine components**

162 **3.2.1 Reconstruction of the terrestrial component**

163 We follow the reconstruction method of CMST-Interim (Sun et al., 2021) and divide the C-
164 LSAT 2.0 dataset into two parts, high- and low-frequency components, for reconstruction, then sum
165 them to obtain the reconstructed LSAT data (Figure 2). The low-frequency component is a running
166 average over time and space to characterize the large-scale features of LSAT anomalies in time and
167 space. First, a 25° x 25° spatial running average is performed, and then the annual average of LSAT
168 anomalies is calculated for at least two months of the year. Then, a 15-year median filter is used for
169 the annual average LSAT, followed by a 15° x 25° spatial sliding average, a 9-point binomial spatial
170 filter, and a 3-point binomial temporal filter for latitude and longitude, respectively, to fill in the
171 default data. Finally, a 15° x 25° spatial running average is applied to latitude and longitude
172 respectively to smooth the spatial distribution of the LSAT. The high-frequency component is the
173 difference between the original data and the low-frequency component, characterizing the local
174 variation of LSAT. We train the EOTs modes using the ERA5 reanalysis dataset (Hersbach et al.,
175 2020) (<https://cds.climate.copernicus.eu/>; last access: July 2020) and localize it. Afterward, the
176 EOTs modes are used to fit the high-frequency data to obtain a full-coverage reconstruction of the
177 high-frequency component (Sun et al., 2021). The reconstructed land temperature data can be
178 obtained by summing the low-frequency and high-frequency components, and finally, the
179 reconstructed data are observationally constrained to remove the low-quality reconstructed data.

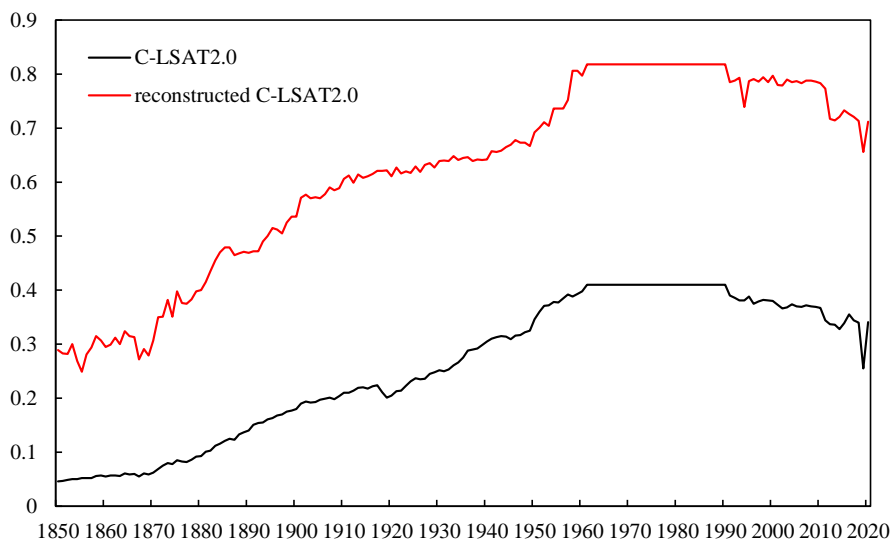
180



181
 182
 183
 184
 185
 186
 187
 188
 189

Figure 2 Schematic diagram of the LSAT reconstruction process

Reconstruction greatly improves the coverage of C-LSAT2.0. Figure 3 shows the comparison of land coverage before and after reconstruction. The land coverage of the reconstructed C-LSAT2.0 increases from the original 4.6% in 1850 to 29%, and the land coverage remains above 60% after 1913 and reaches the maximum land cover of about 80% in 1961, which last until 1990, after which it slightly decreases and remains at about 78%. After 2012 there is a decreasing trend to about 70%, where the land cover in 2019 is the lowest value of 66% for the period 2012-2020, this is related to the lower number of sites in the year.



190

Figure 3 Coverage comparison of the terrestrial component before and after reconstruction

191

192

3.2.2 Reconstruction of the ocean component

193

194

195

196

197

198

3.3 Reconstruction of Arctic ice surface temperature

199

200

201

202

203

204

205

206

207

208

209

210

211

212

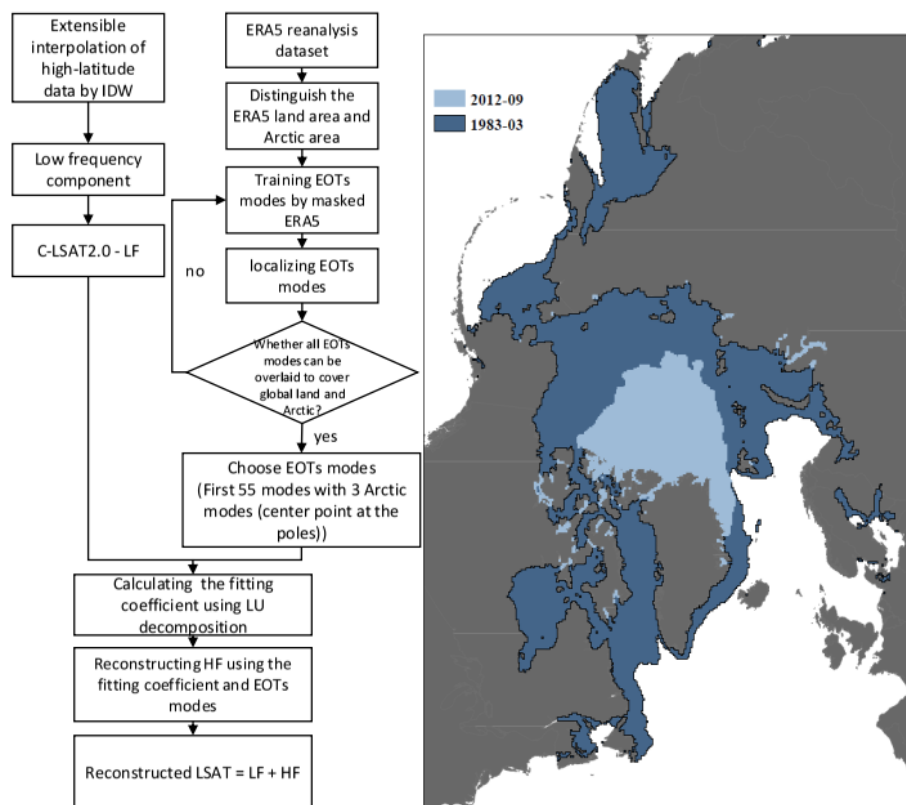
213

214

215

In CMST-Interim, when the Arctic is covered by sea ice, ERSSTv5 sets SST in the region with >90% sea ice coverage to a constant value (-1.8°C), making ST of CMST-Interim in the polar region the default value. It is worth noting that the Arctic is extremely sensitive to changes in climate forcing (polar amplification effect), so missing data in the polar regions in CMST-Interim may lead to an underestimation of the global warming trend (IPCC, 2021).

In order to solve this problem and improve the coverage of CMST in the Arctic, we improve the ST reconstruction method in the Arctic by expressing the ST of the Arctic in terms of the air temperature of ice surface (considering the similar physical properties of ice and land, the sea ice is considered as the land). The month with the largest extent of Arctic sea ice is March, and the month with the smallest extent is September. According to the National Snow and Ice Data Center, during 1980-2020, the year with the largest sea ice extent in March is 1983 and the year with the smallest sea ice extent in September is 2012, so we designed two experiments: 1) CMST2.0-Imax uses 2 m air temperature to represent the temperature within the 65°N-90°N region to simulate the ST of the Arctic sea ice-covered region in March 1983, which is the maximum sea ice extent. 2) CMST2.0-Imin uses 2 m air temperature to represent the temperature within the 80°N-90°N region to represent the ST in the Arctic sea ice-covered region at the time of September 2012, which is the minimum sea ice extent (Figure 4).



216
 217 Figure 4 Reconstruction process of Arctic sea ice ST (left); comparison of maximum sea ice
 218 extent (sea ice extent in March 1983, shaded in dark blue) and minimum sea ice extent(sea ice
 219 extent in September 2012, shaded in light blue) distribution (right)
 220

221 3.3.1 Maximum sea ice extent reconstruction CMST2.0-Imax

222 Due to the scarcity of observations in the Arctic and the fact that most observations were
 223 available after the 1980s, the observation period is very short. The data do not cover all the period
 224 of 1961-1990, which is the climatology of our dataset. Therefore the observations cannot be added
 225 to the C-LSAT 2.0 dataset. Due to this fact, we use the Inverse Distance Weighted method (IDW)
 226 (Cheng et al., 2020) to interpolate the data at lower latitudes to the Arctic (65°N-90°N) and then
 227 perform the high- and low-frequency reconstruction method based on the interpolated dataset. It is
 228 worth noting that we included the region of 65°N-90°N when training EOTs using the ERA5
 229 reanalysis dataset. We selected the first 55 modes of the EOTs with three polar modes (the center
 230 point at the Arctic poles), for a total of 58 modes for reconstructing the high-frequency components
 231 (Figure 4). After that, the reconstructed C-LSAT is merged with ERSSTv5, where the merged
 232 ERSSTv5 covers only the region south of 65°N.

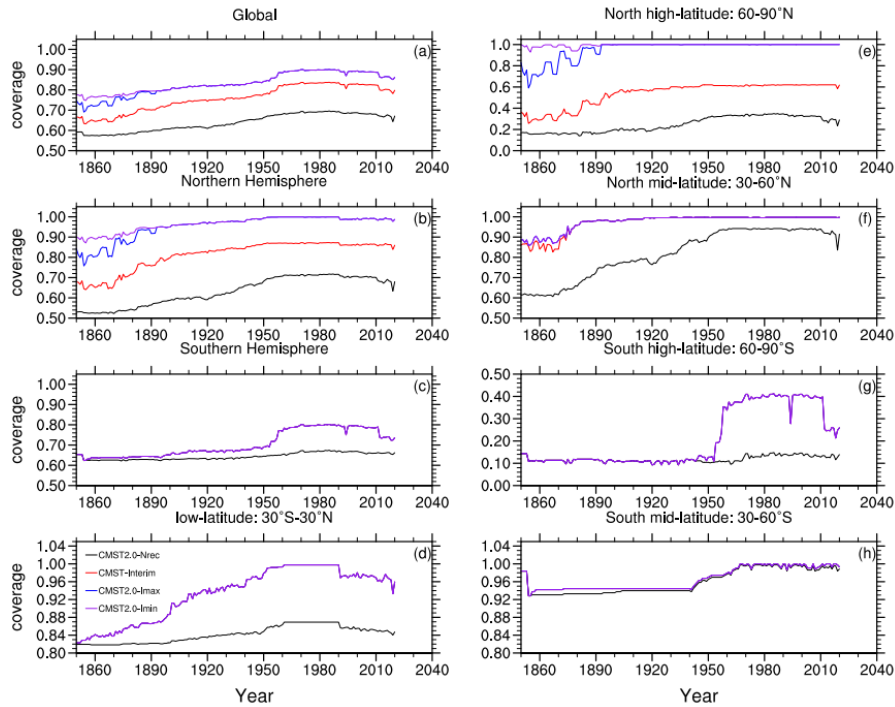
233 3.3.2 Minimum sea ice extent reconstruction CMST2.0-Imin

234 The reconstruction method of the terrestrial component in CMST2.0-Imin is consistent with
 235 CMST2.0-Imax, except that the merged process with ERSSTv5, in CMST2.0-Imin, the merged
 ERSSTv5 coverage is south of 80N. It is worth noting that the sea ice coverage range is 80°N-90°



236 N and the region of 65°N-80°N fill in SST in CMST2.0-Imin. However there are some grids in the
237 region of 65°N-80°N that are default values (caused by sea ice coverage) in ERSSTv5, so we use
238 the IDW method to fill these default grids.

239 Figure 5 shows the coverage comparison of CMST2.0-Nrec (without any land and ice air
240 temperature reconstruction), CMST-Interim, CMST2.0-Imax, and CMST2.0-Imin. Overall, there is
241 a significant improvement in the coverage of the reconstructed datasets compared to the original
242 dataset, CMST2.0-Nrec. Globally, the coverage of CMST2.0-Imax and CMST2.0-Imin
243 reconstructed for Arctic sea ice is consistently higher than CMST-Interim. CMST2.0-Imax and
244 CMST2.0-Imin have the highest global coverage, with >80% coverage after 1899. The global
245 coverage of CMST-Interim reached more than 80% after 1957. The comparative results for Northern
246 Hemisphere coverage are primarily consistent with the global, with CMST2.0-Imax and CMST2.0-
247 Imin having the greatest coverage, both reaching more than 90% after the 1880s, and CMST-Interim
248 reaching 80% coverage in 1901, but consistently below 90%. In terms of global and Northern
249 Hemisphere coverage, there are differences between CMST2.0-Imax, CMST2.0-Imin, and CMST-
250 Interim, but the differences are not significant. However, the coverage of CMST2.0-Imax and
251 CMST2.0-Imin differed significantly from CMST-Interim at high latitudes in the Northern
252 Hemisphere, where the coverage of CMST-Interim has been below 70% due to the existence of sea
253 ice, while CMST2.0-Imax and CMST2.0-Imin reach full coverage at high latitudes in the Northern
254 Hemisphere after 1983. There is no difference in the coverage of the three reconstructed datasets in
255 other regions (Southern Hemisphere, Southern Hemisphere mid-high and low latitudes) except for
256 the Northern Hemisphere and Northern Hemisphere high latitudes. The coverage of the
257 reconstructed dataset in the Southern Hemisphere has improved considerably, with a maximum
258 coverage of about 80%. The coverage of the reconstructed dataset in the high latitudes of the
259 Southern Hemisphere is relatively small, consistently below 50%, due to the scarcity of observations
260 in Antarctica.



261

262 Figure 5 Coverage comparison of CMST2.0-Nrec, CMST-Interim, CMST2.0-Imax and CMST2.0-
 263 Imin

264 **3.4 Estimation of uncertainty in the reconstructed CMST2.0**

265 Uncertainties of the reconstructed CMST2.0 include both land and ocean uncertainties. The
 266 ocean uncertainty is the uncertainty of ERSSTv5. The land uncertainty is based on the reconstructed
 267 C-LSAT2.0 ensemble, which is divided into two parts: parameter uncertainty and reconstruction
 268 uncertainty. Since we reconstruct the temperature of the polar sea ice region in the way that we
 269 reconstruct the LSAT, we calculate the uncertainty of the 65°N-90°N (Imax) and 80°N-90°N (Imin)
 270 regions of CMST2.0-Imax and CMST2.0-Imin following the method of calculating the land
 271 uncertainty.

272 **3.4.1 Parameter uncertainty of C-LSAT2.0 ensemble**

273 In the reconstruction process, we choose different parameters to generate 756-member
 274 ensembles (Table 1), which are different for different combinations, so the parameter uncertainty
 275 represents the difference of parameter combinations. According to Huang et al. (2020), the
 276 parameter uncertainty (U_p) is the regional average LSAT uncertainty, as follows:

$$U_p^2(t) = \frac{1}{M} \sum_{m=1}^M [A_m^g(t) - \bar{A}^g(t)]^2 \quad (1)$$

$$\bar{A}^g = \frac{1}{M} \sum_{m=1}^M A_m^g(t) \quad (2)$$

277 where M is the ensemble member, in this paper $M=756$; A_m^g represents global LSAT of m -member



278 ensemble; $\overline{A^g}$ is the average of all ensembles; t represents temporal variations.

279 Table 1 Parameter settings used for reconstruction scenarios and the operational option.

PARAMETER	OPERATIONAL OPTIONS	ALTERNATIVE OPTIONS
MINIMUM NUMBER OF MONTHS ANNUAL AVERAGE	2 months	1, 2, 3 months
LF FILTER PERIODS	15 years	10, 15, 20 years
MIN NUMBER OF YEARS FOR LF FILTER	2 years	1, 2, 3 years
EOTS TRAINING PERIODS AND SPATIAL SCALES	1979-2018, Lx=4000, 3000, 2500, Ly=2500	1979-2018, Lx=3000,2000,1500, Ly=1500; 1979-2018, Lx=5000,4000,3500, Ly=3500; Lx=4000,3000,2500, Ly=2500; 1979-2008, Lx=4000,3000,2500, Ly=2500; 1989-2018, Lx=4000,3000,2500, Ly=2500; even year, Lx=4000, 3000, 2500, Ly=2500; odd year, Lx=4000, 3000, 2500, Ly=2500;
EOTS ACCEPTANCE CRITERION	0.2	0.10, 0.15, 0.20, 0.25

280 Parameter uncertainties for the reconstructed C-LSAT2.0 ensemble, reconstructed C-
 281 LSAT2.0+Imax (65°N-90°N) and reconstructed C-LSAT2.0+ Imin (80°N-90°N) show similar
 282 variations. The parameter uncertainties decreases over time, as does its interannual variability. The
 283 parameter uncertainties stabilizes below 0.05 during 1876-2016 (Figure 7). However, the parameter
 284 uncertainty is higher in 2018-2020 compared to the previous years. This is due to the lower coverage
 285 in this period compared to the last years, which is more sensitive to the parameter settings.

286 3.4.2 Reconstruction uncertainty of C-LSAT2.0 ensembles

287 In the reconstruction process, we smooth the observations when calculating the low-frequency
 288 component to filter out the short-term and local signals to obtain the large-scale characteristics of
 289 the LSAT anomaly, after which the high-frequency component is used to fit the local distribution of
 290 LSAT using the EOTs spatial modes and the available observations. Our purpose of using EOTs is
 291 to obtain the spatial distribution of the LSAT anomaly, filter out the errors in the observations, and
 292 thus estimate the distribution of the LSAT anomaly from limited observations. However, the spatial
 293 pattern of EOTs also smoothes out the local temperature and ignores some local information, thus
 294 deviating from the observations. Therefore, according to Huang et al. (2016), we define the residual
 295 between the ideal observations and the reconstructed values using EOTs as the reconstruction
 296 uncertainty:

$$U_r^2(t) = \frac{1}{M} \sum_{m=1}^M [R_m^g(t) - D(t)]^2 \quad (3)$$

297 where $D(t)$ represents the ideal observation and $R_m^g(t)$ is the reconstructed data obtained using
 298 the high- and low-frequency reconstruction method based on $D(t)$.

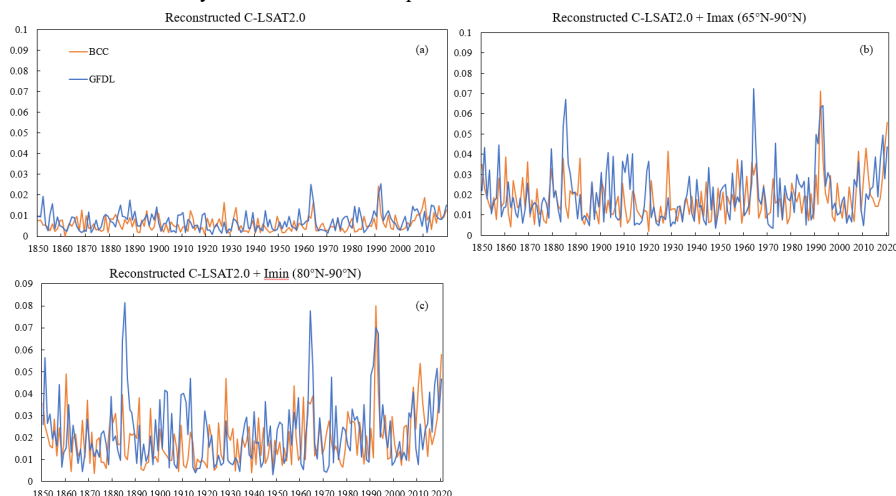
299 The reconstruction uncertainty represents the differences between the ideal observations and
 300 the reconstructions. We choose two full-coverage CMIP6 models to represent the ideal observations
 301 to assess the deviation of the reconstructed values from the original values, which is due to missing
 302 information caused by the smoothing of local temperatures by EOTs. The C-LSAT 2.0 ensemble
 303 dataset covers the period 1850-2020, while the CMIP6 model historical experimental data are only



304 available up to 2014, so we use model data from the SSP370 scenario (taking into account minor
 305 differences in the short term for any scenarios) to complement that of 2015-2020.

306 The two models we selected are BCC-CSM2-MR and GFDL-ESM4. BCC-CSM2-MR is a new
 307 version of the climate system model developed by the National Climate Center of China with
 308 improved parameterization and physical parameterization results. GFDL-ESM4 is an Earth system
 309 model developed by the GFDL model of NOAA's Geophysical Fluid Dynamics Laboratory. Both
 310 models have a resolution of 1.125×1.125 , and we descale both to 5×5 to calculate the temperature
 311 anomaly (1961-1990 climatology), after which the data from both models are reconstructed
 312 according to the high- and low-frequency reconstruction method.

313 Figure 6 shows the reconstruction uncertainties calculated using BCC-CSM2-MR and GFDL-
 314 ESM4. In general, the reconstruction uncertainties are relatively stable, do not increase over time.
 315 The reconstruction uncertainties of reconstructed C-LSAT2.0+Imax and reconstructed C-LSAT2.0+
 316 Imin are larger than that of reconstructed C-LSAT2.0, and the interannual variation is also larger.
 317 The interannual variability of the uncertainty of BCC-CSM2-MR is slightly smaller than that of
 318 GFDL-ESM4. In the following, we choose BCC-CSM2-MR as the reconstruction uncertainty to
 319 discuss the uncertainty of the terrestrial component.



320
 321 **Figure 6** Reconstruction uncertainty of the reconstructed C-LSAT2.0 ensemble,
 322 reconstructed C-LSAT2.0+Imax ($65^{\circ}\text{N}-90^{\circ}\text{N}$) and reconstructed C-LSAT2.0+ Imin ($80^{\circ}\text{N}-90^{\circ}\text{N}$)
 323 calculated using BCC-CSM2-MR and GFDL-ESM4.

324 3.4.3 Total uncertainty of LSAT

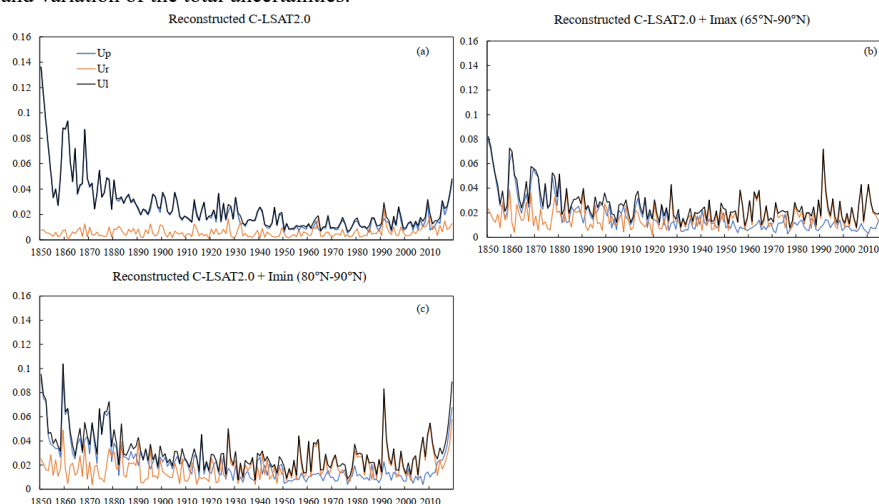
325 The total uncertainty of the C-LSAT2.0 ensemble is the sum of the parameter uncertainty and
 326 the reconstruction uncertainty:

$$U_t^2 = U_p^2 + U_r^2 \quad (4)$$

327 Figure 7 shows the comparison of parameter uncertainty, reconstruction uncertainty and total
 328 uncertainty of three C-LSAT2.0 ensemble datasets. The parameter uncertainties of the reconstructed
 329 C-LSAT2.0 ensemble, reconstructed C-LSAT2.0+Imax ($65^{\circ}\text{N}-90^{\circ}\text{N}$) and reconstructed C-
 330 LSAT2.0+ Imin ($80^{\circ}\text{N}-90^{\circ}\text{N}$) are much larger than the reconstruction uncertainties before 1950,
 331 when the parameter uncertainties mainly determines the magnitude of total uncertainties. The



332 difference between the parameter uncertainties and the reconstruction uncertainties from 1950-2016
 333 becomes small, and both determine the total uncertainties. The total uncertainties increase after 2017
 334 due to the increase in parameter uncertainties (Figure 7a). The uncertainties of reconstructed C-
 335 LSAT2.0+Imax and C-LSAT2.0+Imin vary similarly (Figure 7b&7c). The parameter uncertainties
 336 of reconstructed C-LSAT2.0+Imax and C-LSAT2.0+Imin is larger than the reconstruction
 337 uncertainties before 1880, when the total uncertainties is dependent on parameter uncertainties.
 338 During 1880-1950, the magnitude and variation of the parameter uncertainties and the
 339 reconstruction uncertainties are similar. After 1950, the parameter uncertainties decrease to less than
 340 the reconstruction uncertainties, during which reconstruction uncertainties determine the magnitude
 341 and variation of the total uncertainties.



342
 343 Figure 7 Parameter Uncertainty, reconstruction uncertainty and total uncertainty of three
 344 reconstructed C-LSAT2.0 ensemble

345 3.4.4 Uncertainty of global surface temperature

346 The uncertainty of the global surface temperature consists of two components, the ocean
 347 component and the land component, and we calculate the total global temperature uncertainty as the
 348 sum of the two, based on the sea-to-land ratio, with the following formula:

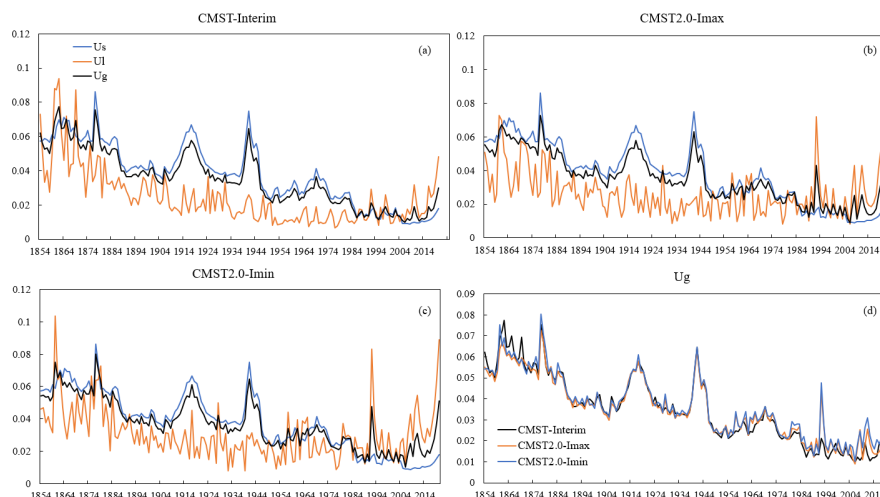
$$U_g^2 = a \times U_l^2 + b \times U_s^2 \quad (5)$$

349 where U_g represents the total uncertainty of GMST, U_l represents the uncertainty of global
 350 averaged LSAT, here chosen from the reconstructed C-LSAT2.0; U_s represents the uncertainty of
 351 global averaged ocean component, here chosen from the ERSSTv5, since the uncertainty of
 352 ERSSTv5 is only calculated up to 1854, our uncertainty of GST forward also only covers up to 1854.
 353 a and b are constants, which are the proportion of land and ocean area to the globe, respectively, but
 354 since the uncertainty of reconstructed Arctic region in CMST2.0+Imax and CMST2.0+Imin is
 355 calculated according to the land uncertainty, $a=0.32$ and $b=0.689$ in CMST2.0+Imax and $a=0.30$ and
 356 $b=0.70$ in CMST2.0+Imin.

357 Figure 8 shows uncertainties of the GMST, land component, and ocean component for CMST-
 358 Interim (a), CMST2.0+Imax (b) and CMST2.0+Imin (c). The variation in GMST uncertainty is
 359 similar for the three datasets, but the interannual variation in GMST uncertainty for CMST2.0+Imax



360 and CMST2.0-Imin is larger than CMST-Interim, especially after 1994, when both the magnitude
361 and interannual variation in GMST uncertainty for CMST2.0-Imax and CMST2.0-Imin are
362 significantly greater than CMST-Interim (Figure 8d). Uncertainties in the ocean and land
363 components have generally declined, and thus the uncertainty of GMST has also reduced (Figure
364 8a-c). Before 1870, the uncertainties of land and ocean component are similar, but the interannual
365 variability of the land uncertainty is greater than that of the ocean. During 1871-1986, the
366 uncertainty in the ocean component is larger than the uncertainty in the land component, and the
367 uncertainty of GMST depended mainly on the uncertainty in the ocean component, and the
368 interannual variability was consistent with the ocean component. There are two peaks in global
369 uncertainty during this period, in the late 1910s and early 1940s, consistent with ocean uncertainty.
370 The peaks in ocean uncertainty are associated with the two world wars, and the uncertainty is larger
371 due to the smaller observation coverage of the SST during the war period (Huang et al., 2020).
372 Between 1986 and 2003, the uncertainty of GMST was determined by both the land and ocean
373 components. After 2003, the magnitude of uncertainty of the ocean component is smaller than that
374 of the land component, and the land component determines the magnitude of the uncertainty of GMST,
375 and the interannual variation is also consistent with the land component.



376
377 Figure 8 Uncertainties of GMST (U_g), LSAT (U_l) and SST (U_s) for CMST-Interim (a), CMST2.0-
378 Imax (b) and CMST2.0-Imin (c) and their comparison of U_g (d).

379 4. Composition of C-LSAT2.0 and CMST2.0

380 The C-LSAT2.0 datasets consist of two datasets, C-LSAT2.0 and reconstructed C-LSAT2.0, while
381 each dataset includes three temperature-related elements, including monthly average, maximum,
382 and minimum temperatures.

383 The CMST2.0 datasets consist of three versions: CMST2.0-Nrec, CMST2.0-Imax, and
384 CMST2.0-Imin.

385 CMST2.0-Nrec is the observation-based homogenized gridded dataset, consisting of C-
386 LSAT2.0 and ERSSTv5, where the uncertainty of C-LSAT2.0 is not estimated, and the uncertainty
387 of ERSSTv5 consists of parameter uncertainty and reconstruction uncertainty.

388 CMST2.0-Imax is based on CMST-Interim gridded dataset with the addition of Arctic
389 reconstruction (65N-90N), including reconstructed C-LSAT2.0 with the addition of Arctic



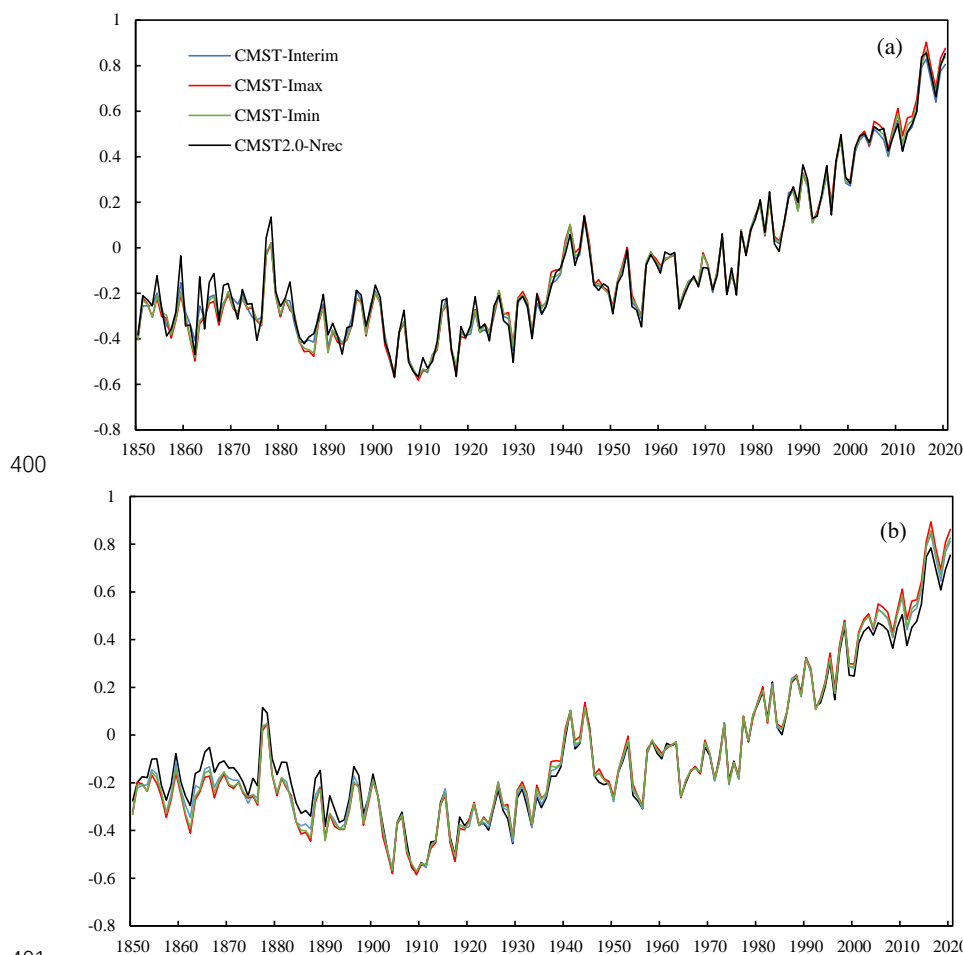
390 reconstruction (65N-90N) and ERSSTv5 with 90S-60N. Its uncertainties include the terrestrial
 391 uncertainty and the oceanic uncertainty, where the terrestrial uncertainty is the uncertainty of the
 392 reconstructed C-LSAT2.0 and of the reconstructed SAT over ice surface, including the parameter
 393 uncertainty and the reconstruction uncertainty, and the oceanic uncertainty is derived from the
 394 uncertainty of ERSSTv5 (Huang et al., 2017).

395 Similarly, CMST2.0-Imin is the gridded data, which modifies the reconstructed Arctic region
 396 based on CMST2.0-Imin. The modification part is to reduce the reconstructed Arctic region of C-
 397 LSAT2.0 to 80N-90N and expand the merged ERSSTv5 to 90S-80N area.

398 Table 2 Composition of CMST2.0 datasets and CMST-Interim.

Versions	Timespan	LSAT		SST	
		datasets	uncertainty	datasets	uncertainty
CMST2.0-Nrec	1850-2020	C-LSAT2.0	—	ERSSTv5	
CMST-Interim	1850-2020	Reconstructed C-LSAT2.0		ERSSTv5	
CMST2.0-Imax	1850-2020	Reconstructed C-LSAT2.0 added Arctic reconstruction (65N-90N)	Parameter uncertainty + Reconstruction uncertainty	ERSSTv5 (90S-65N)	Parameter uncertainty + Reconstruction uncertainty
CMST2.0-Imin	1850-2020	Reconstructed C-LSAT2.0 added Arctic reconstruction (80N-90N)		ERSSTv5 (90S-80N)	

399 **5. The GMST series of CMST2.0 datasets**



400

401

402 Figure 9 Comparison of GMST series for CMST2.0 datasets and CMST-Interim using two
403 methods: a) the mean of global mean LSAT and SST weighted the proportion of land and sea.; b)
404 calculated based on latitudinal weighting

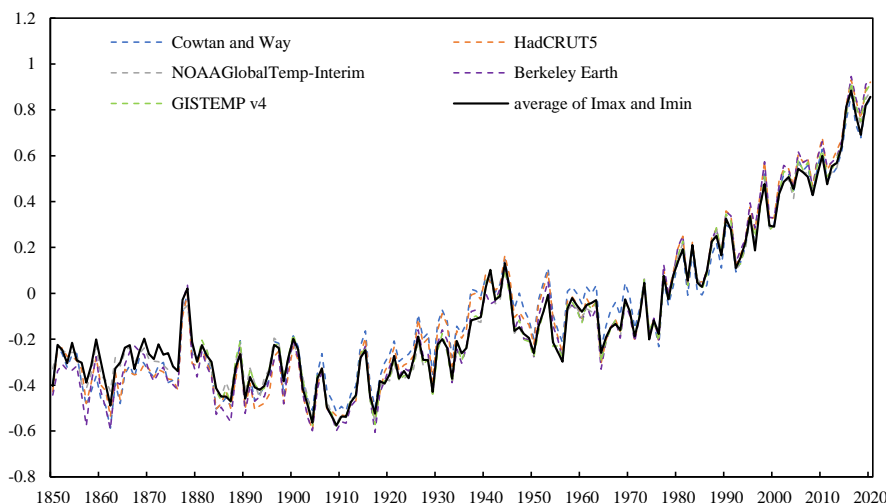
405 Comparing the GMST series of CMST2.0 datasets and CMST-Interim shows that the variability
406 of GMST in the reconstructed datasets is generally consistent with CMST2.0-Nrec (Figure 9). We
407 also compare the GMST series for the four datasets calculated by the two methods, which is similar
408 for the three reconstructed datasets (CMST-Interim, CMST2.0-Imax and CMST2.0-Imin) and differ
409 slightly for the unreconstructed dataset CMST2.0-Nrec (Figure 9a & 9b). The warming of CMST-
410 Nrec in Figure 9b is significantly lower than that that in Figure 9a and , which is related to the lower
411 land coverage. The LSAT coverage of CMST2.0-Nrec was low in previous decades, which is below
412 18% before 1900 (Fig. 3), so the GMST series is susceptible to the influence of ocean temperature,
413 making the GMST series high; The LSAT coverage of CMST2.0-Nrec has increased in recent
414 decades, with terrestrial coverage above 70% (Figure 3), but the coverage is low at high latitudes,
415 in South America and Africa, where the absence of LSAT, especially at high latitudes and in the
416 Arctic, makes the GMST series low. It can be seen that the warming rate of CMST2.0-Nrec



417 calculated using latitude-weighting will be significantly lower, so we are using the sea-land ratio
418 method to calculate the warming trend when comparing each dataset in the following.

419 In Figure 9a, the CMST-Interim, CMST2.0-Imax and CMST2.0-Imin GMST series are lower
420 than CMST-Nrec before the 1880s, which is mainly due to the lower coverage of observations in
421 this period, making the interannual variability of the GMST series in CMST2.0-Nrec larger, while
422 the reconstructed datasets filled in part of the default grids, resulting in higher coverage and thus
423 lower interannual variability of GMST series. The reconstructed datasets show high agreement with
424 the CMST-Nrec temperature series and its interannual variability as the coverage of the observations
425 increased after the 1880s. While the GMST series of CMST2.0-Imax is significantly higher than the
426 other three datasets after the 2000s because CMST2.0-Imax reconstructs the Arctic region and the
427 polar amplification effect of the Arctic significantly increases the GMST series, the GMST series of
428 CMST-Interim and CMST2.0-Imin are essentially the same as CMST-Nrec, but CMST2.0-Imin is
429 slightly higher than CMST-Interim because CMST2.0-Imin fills the 80N-90N region with ice
430 surface temperatures, while CMST-Interim uses SST. The GMST series of CMST2.0-Imax and
431 CMST2.0-Imin are higher than CMST-Interim after 2000, indicating that the influence of polar
432 temperature on global temperature also increases with global warming. In summary, the warming
433 trends of the reconstructed datasets for 1850-2020 are all higher than CMST2.0-Nrec
434 ($0.05 \pm 0.003^\circ\text{C}/10\text{a}$), with CMST2.0-Imax having the most significant warming trend
435 ($0.054 \pm 0.003^\circ\text{C}/10\text{a}$) and CMST2.0-Imin the second largest ($0.053 \pm 0.003^\circ\text{C}/10\text{a}$) (Table 3). The
436 warming trend estimated by CMST-Interim is $0.051 \pm 0.003^\circ\text{C}/10\text{a}$, which is slightly larger than
437 CMST-Nrec, mainly due to the lower temperature series before the 1880s, excluding this period, the
438 warming trend from 1880 to 2020 estimated by CMST-Interim ($0.073 \pm 0.003^\circ\text{C}/10\text{a}$) is consistent
439 with CMST-Nrec ($0.073 \pm 0.004^\circ\text{C}/10\text{a}$) (Table). While the warming trends of CMST2.0-Imax and
440 CMST2.0-Imin are higher than the previous two datasets, $0.076 \pm 0.004^\circ\text{C}/10\text{a}$ and
441 $0.074 \pm 0.003^\circ\text{C}/10\text{a}$ (Table 3), respectively, due to the polar amplification effect.

442 6. Comparison of CMST2.0-Imax and CMST2.0-Imin with other datasets



443
444 Figure 10 Comparison of GMST series for different datasets. The GMST series is the mean of
445 global mean LSAT and SST weighted the proportion of land and sea. The average of Imax and



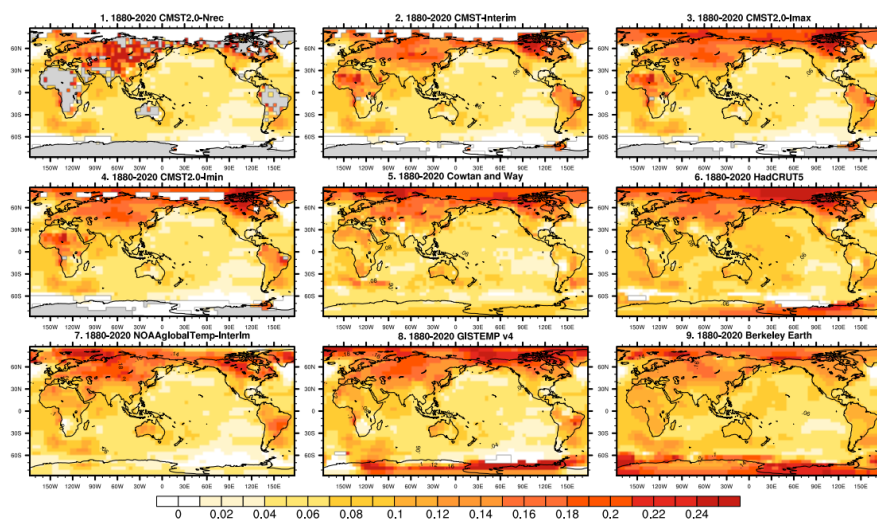
446 Imin is the average of GMST series of CMST2.0-Imax and CMST2.0-Imin.
447
448 Figure 10 shows the GMST series of CMST2.0-Imax and CMST2.0-Imin compared with the
449 other datasets. The GMST series of the seven datasets are generally consistent. The GMST series of
450 CMST2.0-Imax and CMST2.0-Imin are similar to the other five datasets, indicating that their
451 estimated Arctic temperature variation is consistent with the other datasets, and can accurately
452 reflect the impact of the Arctic amplification effect on GST. Due to sparse observations, the
453 variability between datasets is high until the 1880s, as is the interannual variability between datasets.
454 After the 1900s, the GMST series of CMST2.0-Imax and CMST2.0-Imin are generally lower than
455 other datasets. In the 1910s-1970s, the Cowtan-Way dataset is consistently higher than other datasets.
456 In the 1930s-1950s, HadCRUT5 is higher than the other datasets, but similar to Cowtan-Way. After
457 the 2000s, the CMST2.0 datasets are generally lower than other datasets, with CMST2.0-Imax being
458 closer to the NOAAglobalTemp-Interim GMST series. For the period 1850-2020, the warming trend
459 of CMST2.0-Nrec is the lowest ($0.05\pm 0.003^{\circ}\text{C}/10\text{a}$) and the highest ($0.062\pm 0.003^{\circ}\text{C}/10\text{a}$) warming
460 trend is Berkeley in the seven datasets. The warming trend of CMST-Interim is consistent with
461 HadCRUT5, both at $0.051\pm 0.003^{\circ}\text{C}/10\text{a}$. The warming trend of CMST2.0-Imax is the same as
462 NOAAglobalTemp-Interim ($0.054\pm 0.003^{\circ}\text{C}/10\text{a}$). Between 1880 and 2020, CMST2.0-Nrec
463 ($0.073\pm 0.004^{\circ}\text{C}/10\text{a}$) is agreement with CMST-Interim ($0.073\pm 0.003^{\circ}\text{C}/10\text{a}$), CMST2.0-Imax is
464 consistent with NOAAglobalTemp-Interim ($0.076\pm 0.004^{\circ}\text{C}/10\text{a}$), and CMST2.0-Imin
465 ($0.075\pm 0.003^{\circ}\text{C}/10\text{a}$) is consistent with Cowtan -Way ($0.074\pm 0.003^{\circ}\text{C}/10\text{a}$) (Table 3). We also
466 calculate the warming trends of different datasets for different periods 1900-2020, 1951-2020, 1979-
467 2020 and 1998-2020 and found that the warming rate becomes faster over time for most of the
468 datasets, especially the increasing warming trend for 1998-2020 is much larger than the other
469 periods, indicating that the global warming rate is accelerating. The maximum warming trend of
470 $0.228\pm 0.029^{\circ}\text{C}/10\text{a}$ (GISTEMP v4) during 1998-2020 increased by $0.037\pm 0.017^{\circ}\text{C}/10\text{a}$ compared
471 to the warming trend during 1979-2020. the largest increasing warming trend is NOAAglobalTemp-
472 Interim, with a warming trend of $0.037\pm 0.017^{\circ}\text{C}/10\text{a}$ for 1998-2020, which is $0.04^{\circ}\text{C}/10\text{a}$ higher
473 than the warming trend during 1979-2020, followed by CMST2.0-Imax, CMST2.0-Imin and
474 Berkeley Earth, CMST2.0-Nrec and CMST-Interim have relatively small increases in the warming
475 trend. The relatively large increases of warming trend estimated in most datasets with reconstructed
476 Arctic temperatures, compared to those without (CMST2.0-Nrec and CMST-Interim), illustrate the
477 impact of polar amplification on global warming and reflect the importance of reconstructing Arctic
478 default data.



479 Table 3 Warming trends for different datasets during different periods. The GMST series used to
 480 calculate the warming trend is the mean of global mean LSAT and SST weighted the proportion of
 481 land and sea.

	CMST2.0 -Nrec	CMST- Interim	CMST- Imax	CMST-Imin	Cowtan – Way	HadCRUT5	NOAAglobal Temp-Interim	Berkeley Earth	GISTEM P v4
1850-2020	0.050±0.0 03	0.051±0.0 03	0.054±0.00 3	0.053±0.003	0.058±0.003	0.051±0.003	0.054±0.003	0.062±0.0 03	—
1880-2020	0.073±0.0 04	0.073±0.0 03	0.076±0.00 4	0.075±0.003	0.074±0.003	0.081±0.004	0.076±0.004	0.083±0.0 04	0.077±0.0 04
1900-2020	0.091±0.0 04	0.090±0.0 04	0.093±0.00 4	0.091±0.004	0.084±0.004	0.094±0.004	0.093±0.004	0.099±0.0 04	0.095±0.0 04
1951-2020	0.145±0.0 07	0.139±0.0 07	0.146±0.00 7	0.143±0.007	0.130±0.008	0.150±0.008	0.147±0.007	0.155±0.0 08	0.151±0.0 07
1979-2020	0.174±0.0 13	0.168±0.0 11	0.184±0.01 1	0.179±0.011	0.190±0.012	0.193±0.012	0.184±0.012	0.195±0.0 12	0.191±0.0 12
1998-2020	0.198±0.0 30	0.19±0.02 7	0.212±0.02 6	0.209±0.026	0.189±0.028	0.215±0.028	0.224±0.028	0.220±0.0 30	0.228±0.0 29

482
 483



484
 485
 486
 487
 488
 489
 490
 491
 492
 493

Figure 11 Distribution of warming trends estimated from different datasets during 1880-2020.

Figure 11 compares the distribution of warming trends for different datasets for 1880-2020. The distribution of warming trends is relatively consistent among the nine datasets except for the Antarctic, with a zone of high warming values in central Asia and Europe, and northeastern North America. There are large differences among the datasets in the Antarctic region due to the sparse observations. CMST-Interim, CMSR2.0-Imax and CMST2.0-Min have fewer LSATs in the Antarctic due to the sparse observations and observational constraints. Except for CMST2.0-Nrec, the estimated warming trends of the other eight datasets have a clear trend of increasing with latitude in the Northern Hemisphere region. Most datasets assess a significantly higher warming trend in the



494 Arctic (60N-90N) than in the lower latitudes. Except for the CMST2.0-Nrec and CMST-Interim
495 datasets in which Arctic temperature is not available, the magnitude of the estimated Arctic warming
496 trend for 1880-2020 is similar. Still, the warming trends near the poles differ significantly, with more
497 significant warming trends estimated by HadCRUT5 and GISTEMP v4. CMST2.0-Imax,
498 CMST2.0- Imin, Cowtan-Way and Berkeley Earth have similar warming trends, while
499 NOAAglobalTemp-Interim has the smallest warming estimate near the poles. CMST2.0-Imax,
500 HadCRUT5, and GISTEMP v4 all show a high warming trend in the high latitudes of North America
501 and the northwestern Arctic Ocean, but CMST2.0-Imax has a relatively small range of highs.
502 Cowtan-Way and Berkeley Earth are similar to the former three datasets, but with smaller ranges
503 and magnitudes. Meanwhile, each dataset also has a range of warming highs in the southeastern
504 Arctic Ocean, NOAAglobalTemp-Interim estimates the most extensive range of warming,
505 CMST2.0-Imax, CMST2.0-Min, HadCRUT5, and GISTEMP v4 estimate similar ranges of
506 warming. In addition, all datasets, including CMST2.0-Nrec and CMST-Interim, have low warming
507 trend near Scandinavia. The analysis of the warming trends in the Arctic shows that the magnitude
508 and spatial distribution of the warming trends estimated based on CMST2.0-Imax and CMST-Imin
509 are more consistent with the other datasets. Therefore they are reasonable for the spatial
510 interpolation reconstruction of temperature anomalies in the Arctic.

511 7. Summary and Prospects

512 This paper describes the composition and construction process of the latest versions of the C-
513 LSAT 2.0 and CMST 2.0 ensemble datasets. The C-LSAT 2.0 datasets consist of the C-LSAT 2.0
514 gridded dataset and the reconstructed C-LSAT 2.0 dataset, including three meteorological elements:
515 monthly average, maximum and minimum temperatures. The CMST2.0 datasets consist of the
516 CMST 2.0-Nrec gridded dataset and two reconstructed datasets (including CMST 2.0-Imax and
517 CMST2.0-Imin). The CMST 2.0 datasets contain the monthly average temperature anomaly. The
518 resolution of all datasets is 5x5 and the time range is 1850-2020. The reconstructed C-LSAT 2.0
519 dataset, reconstructed according to the high- and low-frequency reconstruction method in Sun et al.
520 (2021), is merged with ERSSTv5 to generate the global surface temperature ensemble dataset
521 CMST-Interim. CMST 2.0-Imax and CMST 2.0-Imin are based on CMST-Interim, combining IDW
522 and high- and low-frequency reconstruction methods for temperature reconstruction in the Arctic.
523 Compared with the unreconstructed dataset CMST 2.0-Nrec, the coverage of the reconstructed
524 datasets is greatly improved. These two datasets have greatly improved coverage in the Northern
525 Hemisphere due to the reconstruction in the Arctic. Compared to 60%-70% for CMST 2.0-Nrec
526 before 1910, the coverage of CMST-Interim has improved to 75%-85%, and CMST 2.0-Imax and
527 CMST 2.0-Imin are both above 80%. The coverage of CMST 2.0-Imax and CMST2.0-Imin in the
528 Northern Hemisphere is 80%-99% and CMST-Interim is 65%-87%. In the Southern Hemisphere,
529 there was no difference in coverage between the three reconstructed datasets.

530 We then systematically evaluate the uncertainty of the reconstructed datasets. The results of
531 the uncertainty assessment of the reconstructed C-LSAT 2.0 show that the magnitude of the
532 reconstruction uncertainty is generally smaller than that of the parameter uncertainty, and the
533 parameter uncertainty mainly determines the total uncertainty of the LSAT. The uncertainty of the
534 reconstructed LSAT is similar to previous estimates (Li et al., 2020; Sun et al., 2021). The
535 uncertainty of reconstructed C-LSAT2.0+Imax and reconstructed C-LSAT2.0+Imin is relatively
536 consistent with the uncertainty variation of reconstructed C-LSAT2.0, but the interannual variation
537 is larger, and the increasing trend of parameter uncertainty of reconstructed C-LSAT2.0+Imax and



538 reconstructed C-LSAT2.0+Imin is significantly higher than that of reconstructed C-LSAT2.0 after
539 2017. The uncertainty analysis of CMST 2.0 shows that the uncertainty of GST depends mainly on
540 the oceanic component before 1986, is determined by both oceanic and terrestrial components
541 during 1986-2003, and depends on the magnitude of the terrestrial component after 2003.

542 Results comparing the GMST series of the three CMST 2.0 datasets and CMST-Interim show
543 that the reconstructed datasets improve the estimation of global warming trends while increasing
544 data coverage, especially for the datasets that include the Arctic region in the reconstructed area.
545 Compared with $0.05 \pm 0.003^{\circ}\text{C}/10\text{a}$ and $0.073 \pm 0.004^{\circ}\text{C}/10\text{a}$ for CMST 2.0-Nrec, CMST 2.0-Imax
546 and CMST 2.0-Imin estimated warming trends of $0.054 \pm 0.003^{\circ}\text{C}/10\text{a}$ and $0.053 \pm 0.003^{\circ}\text{C}/10\text{a}$ for
547 1850 -2020 and 1880 -2020 is $0.076 \pm 0.004^{\circ}\text{C}/10\text{a}$ and $0.075 \pm 0.003^{\circ}\text{C}/10\text{a}$, with a very significant
548 increase. Compared with the five datasets in IPCC AR6, it can be found that the datasets considering
549 the reconstruction of Arctic sea ice temperature can more accurately reflect the effect of polar
550 amplification on global temperature, and the GMST series and warming trends estimated by CMST
551 2.0-Imax and CMST 2.0-Imin are more consistent with these five datasets, and both have similar
552 estimates of the spatial distribution and magnitude of warming trends in the Arctic as the other
553 datasets.

554 The current CMST 2.0 dataset for the Arctic is a reconstruction of the sea ice surface
555 temperature in a defined region (65°N - 90°N or 80°N - 90°N) with 2 meters air temperature. Although
556 the influence of Arctic temperature on global temperature is considered and the change of GMST
557 series is estimated relatively accurately, it still cannot reflect the impact of sea ice dynamics on
558 global temperature very accurately. Therefore, our future work will gradually consider the dynamics
559 of sea ice as much as possible in the reconstruction process in order to more accurately estimate and
560 analyze the amplification effect of the Arctic and its impact on GMST.

561 Last but not the least, due to the limited observations, it is very difficult to fully reconstruct the
562 SATs over the Antarctic and the surrounding SSTs during the earlier periods (for example: prior to
563 1950s), which made the CMST2.0 is still not “fully” coverage. This will need to be better addressed
564 by continuing to supplement data sources and refining technical methods in future studies.

565 8. Data availability

566 The C-LSAT2.0 datasets are currently publicly available at the website of figshare under the DOI
567 <https://doi.org/10.6084/m9.figshare.16968334.v4> (Sun and Li, 2021b), which contains monthly
568 mean, maximum and minimum temperature before and after reconstruction during 1850-2020. The
569 CMST2.0 datasets can be downloaded at <https://doi.org/10.6084/m9.figshare.16929427.v4> (Sun
570 and Li, 2021a), which contains CMST2.0-Nrec, CMST-Interim, CMST2.0-Imax and CMST2.0-
571 Imin datasets.

572
573 **Author contributions.** All co-authors were involved in data collection, data analysis, and dataset
574 development. QL was primarily responsible for writing the paper and constructing the dataset. QL
575 and WS conceived the study design with the participation of all co-authors. All authors were
576 involved in the writing of the paper.

577
578 **Competing interests.** The authors declare that they have no conflict of interest.

579
580 **Acknowledgments.** This study is supported by the Natural Science Foundation of China (Grant:



581 41975105), the National Key R&D Program of China (Grant: 2018YFC1507705;
582 2017YFC1502301).
583
584

585 Reference

- 586 Brohan, P., Kennedy, J. J., Harris, I., Tett, S. F. B., and Jones, P. D.: Uncertainty estimates in regional
587 and global observed temperature changes: A new data set from 1850, *Journal of Geophysical*
588 *Research: Atmospheres*, 111, 2006.
- 589 Cheng, J., Li, Q., Chao, L., Maity, S., Huang, B., and Jones, P.: Development of High Resolution
590 and Homogenized Gridded Land Surface Air Temperature Data: A Case Study Over Pan-East
591 Asia, *Frontiers in Environmental Science*, 8, 2020.
- 592 Cowtan, K. and Way, R. G.: Coverage bias in the HadCRUT4 temperature series and its impact on
593 recent temperature trends, *Quarterly Journal of the Royal Meteorological Society*, 140, 1935-
594 1944, 2014.
- 595 Dai, A., Luo, D., Song, M., and Liu, J.: Arctic amplification is caused by sea-ice loss under
596 increasing CO₂, *Nature Communications*, 10, 2019.
- 597 Freeman, E., Woodruff, S. D., Worley, S. J., Lubker, S. J., Kent, E. C., Angel, W. E., Berry, D. I.,
598 Brohan, P., Eastman, R., Gates, L., Gloeden, W., Ji, Z., Lawrimore, J., Rayner, N. A.,
599 Rosenhagen, G., and Smith, S. R.: ICOADS Release 3.0: a major update to the historical marine
600 climate record, *International Journal of Climatology*, 37, 2211-2232, 2017.
- 601 Goosse, H., Kay, J. E., Armour, K. C., Bodas-Salcedo, A., Chepfer, H., Docquier, D., Jonko, A.,
602 Kushner, P. J., Lecomte, O., Massonnet, F., Park, H.-S., Pithan, F., Svensson, G., and
603 Vancoppenolle, M.: Quantifying climate feedbacks in polar regions, *Nature Communications*,
604 9, 2018.
- 605 Hansen, J., Ruedy, R., Sato, M., and Lo, K.: GLOBAL SURFACE TEMPERATURE CHANGE,
606 *Reviews of Geophysics*, 48, 2010.
- 607 Hersbach, H., Bell, B., Berrisford, P., Hirahara, S., Horányi, A., Muñoz-Sabater, J., Nicolas, J.,
608 Peubey, C., Radu, R., Schepers, D., Simmons, A., Soci, C., Abdalla, S., Abellan, X., Balsamo,
609 G., Bechtold, P., Biavati, G., Bidlot, J., Bonavita, M., De Chiara, G., Dahlgren, P., Dee, D.,
610 Diamantakis, M., Dragani, R., Flemming, J., Forbes, R., Fuentes, M., Geer, A., Haimberger, L.,
611 Healy, S., Hogan, R. J., Hólm, E., Janisková, M., Keeley, S., Laloyaux, P., Lopez, P., Lupu, C.,
612 Radnoti, G., de Rosnay, P., Rozum, I., Vamborg, F., Villaume, S., and Thépaut, J.-N.: The ERA5
613 global reanalysis, *Quarterly Journal of the Royal Meteorological Society*, 146, 1999-2049,
614 <https://doi.org/10.1002/qj.3803>, 2020.
- 615 Huang, B., Thorne, P. W., Smith, T. M., Liu, W., Lawrimore, J., Banzon, V. F., Zhang, H.-M.,
616 Peterson, T. C., and Menne, M.: Further Exploring and Quantifying Uncertainties for Extended
617 Reconstructed Sea Surface Temperature (ERSST) Version 4 (v4), *Journal of Climate*, 29, 3119-
618 3142, 2016.
- 619 Huang, B., Thorne, P. W., Banzon, V. F., Boyer, T., Chepurin, G., Lawrimore, J. H., Menne, M. J.,
620 Smith, T. M., Vose, R. S., and Zhang, H.-M.: Extended Reconstructed Sea Surface Temperature,
621 Version 5 (ERSSTv5): Upgrades, Validations, and Intercomparisons, *Journal of Climate*, 30,
622 8179-8205, 2017.
- 623 Huang, B., Menne, M. J., Boyer, T., Freeman, E., Gleason, B. E., Lawrimore, J. H., Liu, C., Rennie,



- 624 J. J., Schreck, C. J., Sun, F., Vose, R., Williams, C. N., Yin, X., and Zhang, H.-M.: Uncertainty
625 Estimates for Sea Surface Temperature and Land Surface Air Temperature in
626 NOAA GlobalTemp Version 5, *Journal of Climate*, 33, 1351-1379, 2020.
- 627 IPCC, 2013: *Climate Change 2013: The Physical Science Basis. Contribution of Working Group I*
628 *to the Fifth Assessment Report of the Intergovernmental Panel on Climate Change* [Stocker,
629 T.F., D. Qin, G.-K. Plattner, M. Tignor, S.K. Allen, J. Boschung, A. Nauels, Y. Xia, V. Bex and
630 P.M. Midgley (eds.)]. Cambridge University Press, Cambridge, United Kingdom and New
631 York, NY, USA, 1535 pp.
- 632 IPCC, 2021: *Climate Change 2021: The Physical Science Basis. Contribution of Working Group I*
633 *to the Sixth Assessment Report of the Intergovernmental Panel on Climate Change* [Masson-
634 Delmotte, V., P. Zhai, A. Pirani, S.L. Connors, C. Péan, S. Berger, N. Caud, Y. Chen, L. Goldfarb,
635 M.I. Gomis, M. Huang, K. Leitzell, E. Lonnoy, J.B.R. Matthews, T.K. Maycock, T. Waterfield,
636 O. Yelekçi, R. Yu, and B. Zhou (eds.)]. Cambridge University Press. InPress.
- 637 Jones, P. D., Osborn, T. J., and Briffa, K. R.: Estimating Sampling Errors in Large-Scale Temperature
638 Averages, *Journal of Climate*, 10, 2548-2568, 1997.
- 639 Kadow, C., Hall, D. M., and Ulbrich, U.: Artificial intelligence reconstructs missing climate
640 information, *Nature geoscience*, 13, 408-413, 2020.
- 641 Kent, E. C., Kennedy, J. J., Smith, T. M., Hirahara, S., Huang, B., Kaplan, A., Parker, D. E., Atkinson,
642 C. P., Berry, D. I., and Carella, G.: A call for new approaches to quantifying biases in
643 observations of sea surface temperature, *Bulletin of the American Meteorological Society*, 98,
644 1601-1616, 2017.
- 645 Latonin, M. M., Bashmachnikov, I. L., Bobylev, L. P., and Davy, R.: Multi-model ensemble mean
646 of global climate models fails to reproduce early twentieth century Arctic warming, *Polar*
647 *Science*, 100677, 2021.
- 648 Lenssen, N. J. L., Schmidt, G. A., Hansen, J. E., Menne, M. J., Persin, A., Ruedy, R., and Zyss, D.:
649 Improvements in the GISTEMP Uncertainty Model, *Journal of Geophysical Research:*
650 *Atmospheres*, 124, 6307-6326, 2019.
- 651 Li, Q., Sun, W., Huang, B., Dong, W., Wang, X., Zhai, P., and Jones, P.: Consistency of global
652 warming trends strengthened since 1880s, *Science Bulletin*, 65, 1709-1712, 2020.
- 653 Li, Q., Sun, W., Yun, X., Huang, B., Dong, W., Wang, X. L., Zhai, P., and Jones, P.: An updated
654 evaluation of the global mean land surface air temperature and surface temperature trends
655 based on CLSAT and CMST, *Climate Dynamics*, 56, 635-650, 2021.
- 656 Lu, J. and Cai, M.: Seasonality of polar surface warming amplification in climate simulations,
657 *Geophysical Research Letters*, 36, 2009.
- 658 Lu, J. and Cai, M.: Quantifying contributions to polar warming amplification in an idealized coupled
659 general circulation model, *Climate Dynamics*, 34, 669-687, 2010.
- 660 Menne, M. J., Williams, C. N., Gleason, B. E., Rennie, J. J., and Lawrimore, J. H.: The global
661 historical climatology network monthly temperature dataset, version 4, *Journal of Climate*, 31,
662 9835-9854, 2018.
- 663 Morice, C. P., Kennedy, J. J., Rayner, N. A., and Jones, P. D.: Quantifying uncertainties in global
664 and regional temperature change using an ensemble of observational estimates: The
665 HadCRUT4 data set, *Journal of Geophysical Research: Atmospheres*, 1, 1-13, 2012.
- 666 Morice, C. P., Kennedy, J. J., Rayner, N. A., Winn, J. P., Hogan, E., Killick, R. E., Dunn, R. J. H.,
667 Osborn, T. J., Jones, P. D., and Simpson, I. R.: An updated assessment of near-surface



- 668 temperature change from 1850: the HadCRUT5 dataset (in press), *Journal of Geophysical*
669 *Research (Atmospheres)*, 2021.
- 670 Parker, D. E.: A demonstration that large-scale warming is not urban, *Journal of climate*, 19, 2882-
671 2895, 2006.
- 672 Parker, D. E., Jones, P. D., Folland, C. K., and Bevan, A.: Interdecadal changes of surface
673 temperature since the late nineteenth century, *Journal of Geophysical Research: Atmospheres*,
674 99, 14373-14399, 1994.
- 675 Rohde, R., Muller, R., Jacobsen, R., Perlmutter, S., Rosenfeld, A., Wurtele, J., Curry, J., Wickham,
676 C., and Mosher, S.: Berkeley earth temperature averaging process, *Geoinformatics &*
677 *Geostatistics: An Overview*, 1, 1-13, 2013a.
- 678 Rohde, R., Muller, R. A., Jacobsen, R., Muller, E., Perlmutter, S., Rosenfeld, A., Wurtele, J., Groom,
679 D., and Wickham, C.: A New Estimate of the Average Earth Surface Land Temperature
680 Spanning 1753 to 2011, *Geoinfor Geostat: An Overview*, 1, 1-7, 2013b.
- 681 Rohde, R. A. and Hausfather, Z.: The Berkeley Earth Land/Ocean Temperature Record, *Earth*
682 *System Science Data*, 12, 3469-3479, 2020.
- 683 Sun, W. and Li, Q.: China global Merged surface temperature 2.0 during 1850-2020,
684 10.6084/m9.figshare.16929427.v4, 2021a.
- 685 Sun, W. and Li, Q.: China global Land Surface Air Temperature 2.0 during 1850-2020,
686 10.6084/m9.figshare.16968334.v4, 2021b.
- 687 Sun, W., Li, Q., Huang, B., Cheng, J., Song, Z., Li, H., Dong, W., Zhai, P., and Jones, P.: The
688 Assessment of Global Surface Temperature Change from 1850s: The C-LSAT2.0 Ensemble
689 and the CMST-Interim Datasets, *Advances in Atmospheric Sciences*, 38, 875-888, 2021.
- 690 Thorne, P. W., Willett, K. M., Allan, R. J., Bojinski, S., Christy, J. R., Fox, N., Gilbert, S., Jolliffe,
691 I., Kennedy, J. J., Kent, E., Tank, A. K., Lawrimore, J., Parker, D. E., Rayner, N., Simmons, A.,
692 Song, L., Stott, P. A., and Trewin, B.: Guiding the Creation of A Comprehensive Surface
693 Temperature Resource for Twenty-First-Century Climate Science, *Bulletin of the American*
694 *Meteorological Society*, 92, ES40-ES47, 10.1175/2011bams3124.1, 2011.
- 695 Trewin, B. C.: Techniques involved in developing the Australian Climate Observations Reference
696 Network – Surface Air Temperature (ACORN-SAT) dataset, CAWCR Technical Report 49,
697 Centre for Australian Weather and Climate Research, Melbourne, 2012.
- 698 Vose, R. S., Huang, B., Yin, X., Arndt, D., Easterling, D. R., Lawrimore, J. H., Menne, M. J.,
699 Sanchez Lugo, A., and Zhang, H. M.: Implementing Full Spatial Coverage in NOAA’s Global
700 Temperature Analysis, *Geophysical Research Letters*, 48, 2021.
- 701 Vose, R. S., Arndt, D., Banzon, V. F., Easterling, D. R., Gleason, B., Huang, B., Kearns, E.,
702 Lawrimore, J. H., Menne, M. J., and Peterson, T. C.: NOAA’s merged land–ocean surface
703 temperature analysis, *Bulletin of the American Meteorological Society*, 93, 1677-1685, 2012.
- 704 Xiao, H., Zhang, F., Miao, L., Liang, X. S., Wu, K., and Liu, R.: Long-term trends in Arctic surface
705 temperature and potential causality over the last 100 years, *Climate Dynamics*, 55, 1443-1456,
706 2020.
- 707 Xu, W., Li, Q., Jones, P., Wang, X. L., Trewin, B., Yang, S., Zhu, C., Zhai, P., Wang, J., Vincent, L.,
708 Dai, A., Gao, Y., and Ding, Y.: A new integrated and homogenized global monthly land surface
709 air temperature dataset for the period since 1900, *Climate Dynamics*, 50, 2513-2536, 2018.
- 710 Yamanouchi, T.: Early 20th century warming in the Arctic: A review, *Polar Science*, 5, 53-71, 2011.
- 711 Yun, X., Huang, B., Cheng, J., Xu, W., Qiao, S., and Li, Q.: A new merge of global surface



712 temperature datasets since the start of the 20th century, Earth System Science Data, 11, 1629-
713 1643, 2019.
714 Zhang, H. M., Lawrimore, J., Huang, B., Menne, M. J., Yin, X., Sánchez-Lugo, A., Gleason, B. E.,
715 Vose, R., Arndt, D., and Rennie, J. J.: Updated temperature data give a sharper view of climate
716 trends, Eos, 100, 1961-2018, 2019.
717